Acta Materialia 147 (2018) 1–9

Contents lists available at ScienceDirect

Acta Materialia

journal homepage: www.elsevier.com/locate/actamat

Full length article

Core structure and solute strengthening of second-order pyramidal $\langle c+a \rangle$ dislocations in Mg-Y alloys

D. Buey [a], L.G. Hector Jr. [b], M. Ghazisaeidi [a, *]

[a] Department of Materials Science and Engineering, Ohio State University, Columbus, OH 43210, USA
[b] General Motors Global R & D, Warren, MI 48092-2031, USA

ARTICLE INFO

Article history:
Received 31 July 2017
Received in revised form
14 December 2017
Accepted 15 December 2017
Available online 11 January 2018

Keywords:
Mg alloys
Pyramidal slip
Density functional theory

ABSTRACT

The ability of Y as an alloying agent to improve the ductility of magnesium is explored using a solid solution strengthening model to determine the relative strengthening effect on the available deformation modes. We use density functional theory calculations to determine the interaction energy between an edge $\langle c+a \rangle$ dislocation and solute atoms surrounding it. We observe that substituting solute atoms directly into the positions closest to the dislocation significantly changes the structure of the dislocation, making the direct calculation and representation of these interaction energies difficult, and necessitating a modification to the calculation of interaction energies. Next, we apply a solution strengthening model to calculate the relative strengthening effect of the solutes and find that the ratio of the critical resolved shear stress of second-order pyramidal $\langle c+a \rangle$ slip to that of the basal slip, decreases with increasing Y concentration. The resulting, more isotropic plastic response is beneficial for improving the room temperature ductility of Mg alloys.

1. Introduction

The high strength to weight ratio of magnesium makes it an attractive material for structural applications in automotive and aerospace industries. However its use as a wrought material has been severely limited by its low room temperature ductility, a consequence of the anisotropic response of its hexagonal close packed (HCP) crystal structure. The critical resolved shear stress (CRSS) required to move dislocations along the basal slip plane (the preferred slip plane in Mg) are more than an order of magnitude lower than the CRSS for non-basal prismatic and pyramidal slip planes [1]. As a result, basal slip dominates deformation under general loading of polycrystalline Mg, and not enough non-basal slip systems are activated to provide the five independent slip systems required by the von Mises criterion for ductility [2]. The addition of alloying elements, capable of modifying the CRSS of various deformation modes, can potentially promote non-basal deformation modes by reducing the critical stress differential between basal and non-basal deformation modes to increase ductility at room temperature. Recent computational work, based on first-principles calculations, has begun to establish a quantitative, theoretical basis to predict the effects of solutes on basal slip [3,4], the twinning mode [5] and the thermally activated basal to prism cross–slip behavior [6,7] in Mg. Despite these advances, a quantitative study of solute effects on the $\langle c+a \rangle$ slip mode does not yet exist. In this paper, we use DFT calculations to compute the $\langle c+a \rangle$ dislocation-solute core structure and interaction energies for Y solutes. We then use these energies to predict the strengthening effect of Y on the pyramidal II glide of $\langle c+a \rangle$ edge dislocations via the modified-Labusch-type strengthening model proposed by Leyson et al. [4]. Yttrium was chosen as an alloying element because it has experimentally been shown to improve the ductility of magnesium without sacrificing strength [8].

Existing DFT-based solute strengthening predictions start with an interaction energy map between the solute and the dislocation. Such maps show the energy of the dislocation, with the solute at various positions in or between the partials, relative to some reference energy configuration. The definition of the reference state is not unique; Yasi et al. used the average of two site energies away from the core, while Leyson et al., used the average energy of all considered sites [3,4]. A well defined interaction energy map relies on the fact that the dislocation core geometry remains unchanged as solutes are placed at various positions. Alternatively, Yasi et al. approximated the solute/dislocation interaction energy based on

* Corresponding author.
E-mail address: ghazisaeidi.1@osu.edu (M. Ghazisaeidi).

https://doi.org/10.1016/j.actamat.2017.12.066
1359-6454/

volume and chemical misfits. This method uses the exact core geometry of the dislocation without any solutes for the accurate changes in bond angles and lengths as well as local volumetric strains inside the core. Volume and stacking fault misfits are then calculated for each solute, using smaller more tractable DFT calculations that do not involve the dislocation directly. The results compare well against direct calculations for Al solutes interacting with basal dislocations in Mg [9]. We find that Y distorts the $\langle c+a\rangle$ dislocation core structure in Mg. Therefore, none of the above methods is directly applicable to our study in their original form. We propose a modification to the misfit approach to take into account the changing core structure of the dislocation as the solute is placed in different positions.

The rest of this paper is organized as follows. The computational techniques and geometries are presented in Section II. In Section III we show and discuss how Y solutes change the core structure of the $\langle c+a\rangle$ dislocation. In section IV we propose a method to compute the solute/dislocation energy map based on a modification to the Yasi et al. [3] misfit energy approach. In Section V, we apply the calculated interaction energies to a solid solution strengthening (SSS) model to determine the relative strengthening effects on basal vs. pyramidal slip and discuss the results.

2. Computational method

The dislocation geometry, used to study the dislocation-solute interactions, is based on previous DFT calculations of the $\langle c+a\rangle$ edge dislocation [10]. The dislocation cell is oriented so that the glide plane coincides with the xz-plane. The cell is periodic along the z-axis, which coincides with the line direction, $[10\bar{1}0]$, and is two repeat units thick along this direction in order to avoid solute-solute interactions. The corresponding k-mesh used was $1\times1\times4$. After substituting selected atoms in the dislocation with yttrium solutes, the cells were again allowed to relax until forces within the cell were below 5 meV/Å. Calculations were performed using the plane-wave DFT code VASP [11,12] using Vanderbilt ultrasoft pseudopotentials and the Perdew-Wang GGA exchange-correlation potential [13]. The energy cutoff was set at 1.3 times the largest of the suggested cutoffs for the potentials, changed accordingly when solute atoms are added. Specific k-meshes are described below for each type of calculation performed.

The size misfit, ε_b, quantifies the difference in size between the solute and host atoms. Calculating the size misfit directly using DFT volume relaxations of an Mg supercell containing a single solute atom gives inconsistent results between different cell sizes. To get a more consistent value, we use the method proposed by Vannarat et al. [14]. Bulk supercells of Mg containing one, two, and three solute atoms are fully relaxed and the resulting changes in pressure are calculated with DFT. The pressure varies linearly with solute concentration, and the size misfit can be calculated using the slope of the pressure vs. solute concentration:

$$\varepsilon_b = \left(\frac{1}{B}\frac{\partial p}{\partial c}\right) \tag{1}$$

where B is the DFT-calculated bulk modulus of pure Mg. These calculations are typically done using supercells made up of $3\times3\times3$ and $4\times4\times4$ bulk unit cells; however, the large misfit between Y and Mg results in a large difference between these values, necessitating larger supercells. Good agreement was seen when using $5\times5\times5$ and $6\times6\times6$ supercells, and the size misfit is taken as the average of those two values. Using this method, the size misfit was found to be 0.576, in good agreement with literature values [15].

The chemical misfit is defined as the logarithmic derivative of the Pyramidal II stacking fault energy γ_{P2} with respect to solute concentration in the dilute range,

$$\varepsilon_{SFE} = \left.\frac{d\ln\gamma_{P2}}{dc_s}\right|_{c_s\approx0} = \frac{1}{\gamma_{P2}}\left.\frac{d\gamma_{P2}}{dc_s}\right|_{c_s\approx0}. \tag{2}$$

Following the methodology described in Ref. [3], we calculate the chemical misfit by creating a $2\times2\times17$ Mg supercell (with a corresponding k-mesh of $8\times8\times1$), resulting in a stack of 17 Pyramidal II planes. The lattice vector perpendicular to the stacking fault plane is tilted in the direction of the lattice vectors in the SF plane in order to create a periodic structure of stacking faults separated by about 40 Å. A solute atom is substituted onto a site in the cell near the stacking fault, and the atoms are allowed to relax until all forces are less than 5 meV/Å. The chemical misfit is calculated from these as:

$$\varepsilon_{SFE} = \frac{E_{SF}(solute) - E_{SF}(Mg)}{\gamma_{P2}\left(\sqrt{3}\,a\right)\left(\sqrt{a^2+c^2}\right)} \tag{3}$$

where the terms in the denominator represent the stable Pyramidal II stacking fault energy per unit area and the area of the Pyramidal II stacking fault. The solute term in the numerator is found by subtracting the total energy of the cell without the stacking fault (but still containing the solute) from the total energy of the cell containing the SF and a solute. The Mg term in the numerator is the total energy of the same stacking fault without the solute atom. This isolates the change in SF energy with the addition of a solute.

Determining the interaction energy between the solute and staking fault for this calculation is not trivial. A recent study by Yin et al. [15] has shown that the pyramidal stacking fault will migrate with the addition of yttrium solutes, making it difficult to determine what the interaction energy is for a solute positioned a few atomic layers away from the SF. The authors work around this by imposing constraints on atoms near the SF to keep it from moving, and find that the SF-solute interaction energy goes to zero several atomic layers away from the fault. In order to accurately represent this, we use a different misfit value for each atomic layer above and below the stacking fault using the stacking fault-solute interaction energies reported in Ref. [15]. This gives values for ε_{SFE} of −0.2775, −0.1526, and −0.0555 for solutes one, two, and three atomic layers away from the stacking fault. These values are unitless, since these values represent the total interaction energy normalized by the pure stacking fault energy.

3. Dislocation core geometry and effect of Y solutes

We start with the geometry of the $\langle c+a\rangle$ edge dislocation in pure Mg, previously calculated by DFT [10]. Fig. 1a shows the Nye density distribution, computed following the method of Hartley and Mishin [16]. The $\langle c+a\rangle$ dislocation dissociates into two $1/2\langle c+a\rangle$ partial dislocations separated by a stacking fault on the pyramidal II plane. A Y solute then substitutes a Mg atom at several locations within the dislocation core and the atomic positions are further optimized to accommodate the presence of the solute. The atomic sites in which solutes are substituted are outlined with bold circles in Fig. 1a. Beyond this region of substituted atoms, the interaction energy is determined using the continuum approximation. The interaction energies are interpolated for a layer of atoms between this outer region and the core where the solutes are substituted in order to ensure a smooth transition.

We observe significant changes to the dislocation core as Y solutes are introduced. Selected core structures, modified in the presence of Y solutes, are shown in Fig. 2. The figure plots the strain along the line direction ε_{zz} for the sake of easy comparison of the

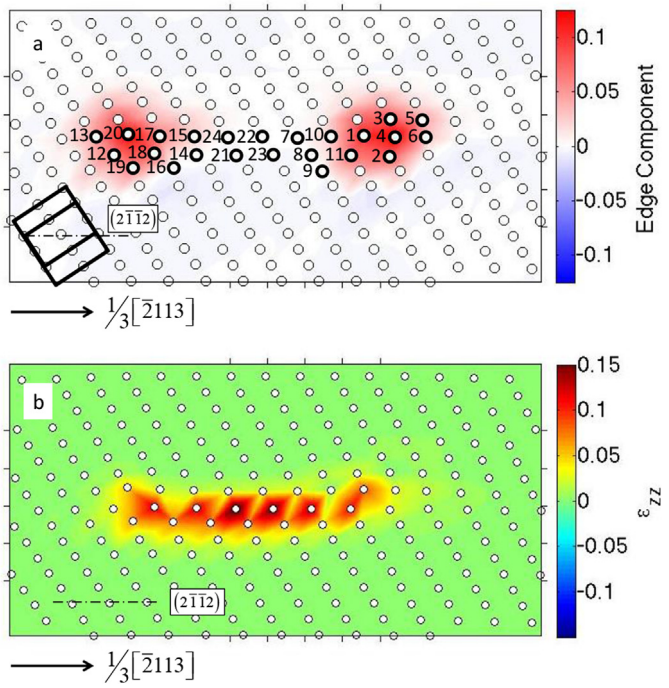

Fig. 1. Dislocation core geometry in pure Mg. The top plot shows the edge component of the corresponding Nye tensor distribution. The atoms outlined in bold indicate the positions of those Mg atoms that are replaced with Y for direct calculations. The bottom plot shows normal strain along the line direction of the dislocation. Beyond the immediate dislocation core region, this strain is zero, making it easy to visualize and compare the size and shape of the dislocations.

exact extent of the dislocation core. This component of the strain is zero outside of the core region and is thus used to clarify changes to the extent of the dislocation core, when solutes are placed at various locations. Part (b) of Fig. 1 shows the ε_{zz} plot for the dislocation in pure Mg, for comparison. Fig. 3 summarizes the changes to the distance between the partials for all solute positions.

It is apparent that some solutes change the shape of the dislocation core and the separation of the partial dislocations significantly. The separation distance between the partials can both increase or decrease depending on the location of the solutes within the dislocation core. Moreover, in some cases, visible distortions are introduced to the atom columns near the solute, with the atoms being shifted so that they no longer align along *z*. This is seen to some extent for each of the solute positions shown in Fig. 2, but is most evident for solutes 15, 16, and 20 in parts (f-h). *The fact that the core structure of the* $\langle c+a \rangle$ *dislocation changes substantially in the presence of Y solutes at various locations inside the core is the first new result of this paper.*

The application of solute strengthening models relies on accurate dislocation/solute interaction energies. In the dilute solution limit, the general picture is that an initially straight dislocation in a field of randomly distributed solutes will bow and shift in order to reach a favorable solute environment that decreases its energy. The total energy change as the dislocation moves from the straight to the bowed out configuration is the sum of the decrease in potential energy resulting from these favorable solute/dislocation interactions and the increase in elastic energy as bowing out increases the length of the dislocation. Therefore, for a dislocation centered at the origin, the key quantity is the interaction energy with solutes at all positions in space, measured from the dislocation core.

Previous DFT studies of solute strengthening have found that the atomic relaxations after introducing a solute atom are small enough that the core structure of the dislocation effectively remains unchanged. However, the large changes seen in the Mg $\langle c+a \rangle$ dislocation structure pose a challenge to a well-defined representation of the interaction energy map. First, while direct DFT calculations of solutes within the dislocation core provide the total energy corresponding to each solute position, the definition of a reference state is not straightforward. Consider a case in which the separation between the partials has changed. While the change occurs as a result of the interaction with the solute, the energy of the dislocation itself, excluding the solute, is now changed. We consider all these energy changes as part of the "interaction" energy. However, this energy must be compared to that of a reference state of the initial dislocation core with a Y solute, far enough from the dislocation, to leave the core structure unchanged. This requires a simulation size significantly larger than the scope of our calculations.

In addition, the change in core geometry leads to difficulty in representing a one-to-one map between the atom positions, relative to the initial dislocation, and atom positions relative to the changing core structure. For instance, consider solute position 3 in Fig. 1a where the left partial does not change, but the right partial dislocation shifts to the right in response to the solute, increasing the separation between the partials. The new relative position of the solute and dislocation is different from that before the relaxation. Therefore, the energy of the relaxed cell cannot be attributed to position 3. In other words, it is not possible to directly compute the solute/dislocation interaction energy at position 3, because once the solute is placed in this position the core structure changes.

To overcome this problem, we use the misfit approximation with some modifications as follows. The misfit approximation approach computes the interaction energy from the local distortions in the dislocation core combined with volumetric and chemical misfits associated with each solute, without the need for a dislocation/solute reference state. However, the original misfit model uses the dislocation core in pure Mg to describe the local environment even in the presence of a solute. Here, we assign a "new" dislocation core to each solute position, and use it to define the local environment and determine the interaction energy for each solute position from the initial core. With this approach, all changes to the dislocation core are considered in the "interaction energy" and assigned to the corresponding solute position that creates that new core. Next, we describe this approach in detail.

4. Calculation of dislocation/solute interaction energy

The misfit approximation, proposed by Yasi et al., describes the dislocation/solute interaction energy in terms of the work done by the dislocation displacement field as well as local shifts to the nearest-neighbor bonds inside the core, on solute "misfits". The solute misfit quantifies the changes to the host lattice upon substitution of solutes and has two major components: size and chemical misfits. The size misfit is caused by the change in local volume as a result of different sizes between the solute and host atoms. The "chemical" misfit accounts for the change in energy to slip the crystal in the presence of the solute. The total interaction energy is given by

$$U = -3BV_0 \cdot e_V \cdot \varepsilon_b + E_{slip} \cdot \varepsilon_{SFE} \tag{4}$$

where ε_b and ε_{SFE} are the solute volume and stacking fault misfits, respectively, V_0 is the equilibrium volume of the Mg supercell used in calculation of the size misfit and B is the bulk modulus for single crystal Mg. Although the single crystal bulk modulus has been shown to change with solute concentration, since we are

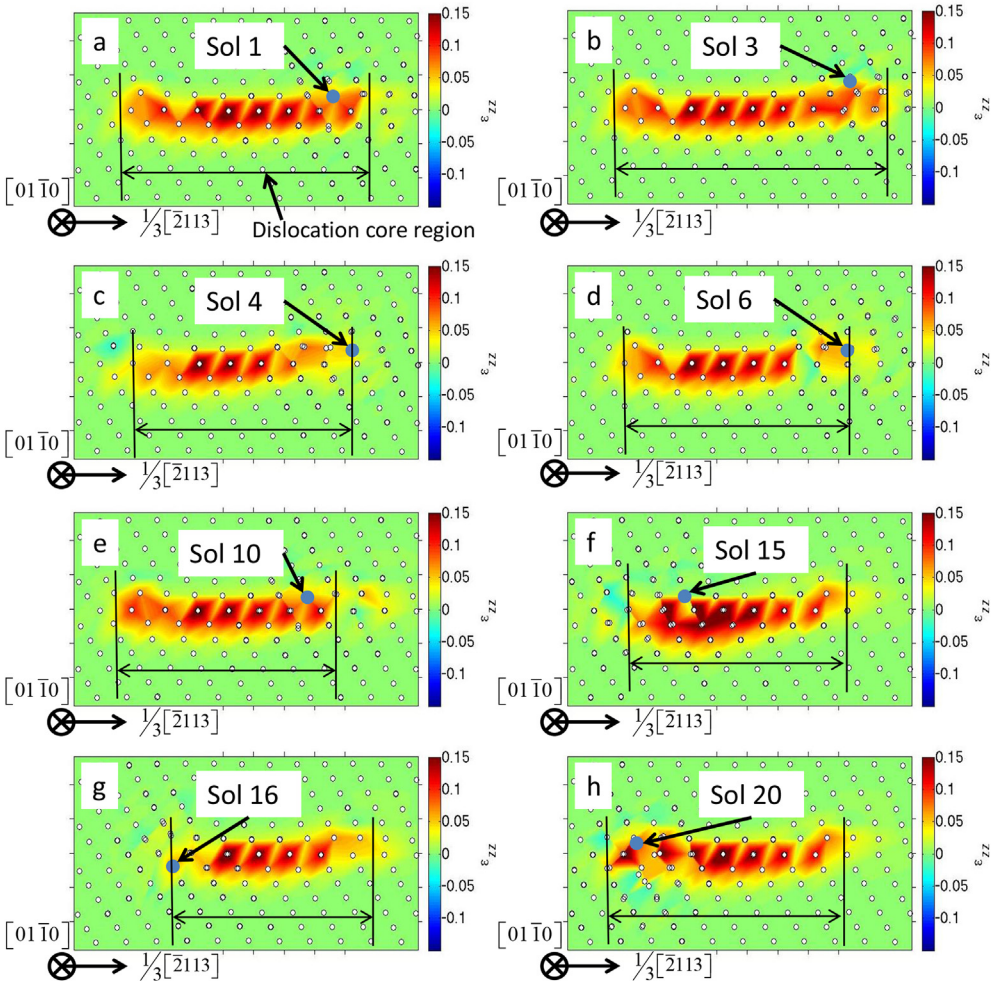

Fig. 2. These plots show the strain along the line direction for the relaxed $\langle c+a \rangle$ edge dislocation after a solute has been added and the dislocation has been relaxed. These cells are oriented so that the $[01\bar{1}0]$ is perpendicular to the plane of the paper. Marks have been added to compare the movement/shape change of the dislocation after each solute has been added. Notice the significant distortion of atomic rows around the solute, with atoms in a single row being shifted so that they no longer overlap. This distortion, which we account for in our model as a change in local volumetric strain, is how the solute atoms change the interaction energy calculation.

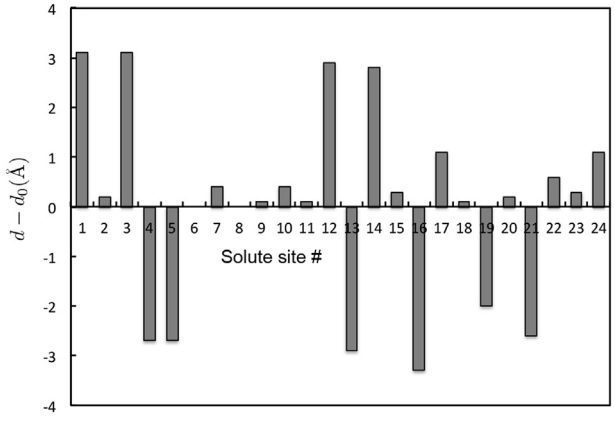

Fig. 3. Difference between the separation between the partials in the presence of Y solute d and that in pure Mg d_0 for all solute locations, corresponding to the positions indicated in part (a) of Fig. 1. Solutes both increase and decrease the separation between the partial dislocations depending on their location inside the dislocation core.

considering a dilute case we ignore this and use the pure Mg modulus. The e_V term is the local volumetric strain at each atomic site, defined relative to the perfect-lattice nearest-neighbor positions as

$$e_V = \left[\frac{det\{\sum_{\vec{x}'} x_i' x_j'\}}{det\{\sum_{\vec{x}} x_i x_j\}}\right]^{\frac{1}{2}} - 1 \tag{5}$$

where $\vec{x'}$ are the vectors to the nearest neighbors for an atomic site in the relaxed dislocation, and $\vec{x}$ are the corresponding nearest-neighbor vectors in a perfect HCP lattice [16]. The E_{slip} term is the slip interaction energy at each atomic site,

$$E_{slip} = \frac{\left(\sqrt{3}\,a/2\right)\cdot\sqrt{a^2+c^2}}{10}\sum_{\vec{d}} \gamma_{(11\bar{2}2)}\left(\vec{d}\right) \tag{6}$$

where $\vec{d}$ represents the vectors to nearest neighbors out of the stacking fault plane, $\gamma_{(11\bar{2}2)}$ is the generalized pyramidal II stacking fault energy corresponding to displacement $\vec{d}$, and the factor of $\frac{1}{10}$ comes from considering one-half of the bond energy of five bonds (determined by considering how many nearest neighbors lie outside of the pyramidal II plane) that would be broken during slip [3]. The slip interaction terms are modified for $\langle c+a \rangle$ slip. It is

important to note that for pyramidal II $\langle c+a\rangle$ dislocations, the local slip environment must be examined carefully. Recent studies have shown that the pyramidal stacking fault can migrate or spread over several atomic layers [17]. In order to address this, we consider the slip environment around several layers of atoms above and below the dislocation. For the case of our dislocations, the stacking fault stayed on the same atomic plane (i.e. the slip across the two atomic planes between the partial dislocations remains close to $\frac{1}{2}\langle c+a\rangle$), though there was still some slight shifting of the atoms directly above and below the stacking fault. These shifts were not necessarily in the plane of the stacking fault, but are still taken into account when considering the volumetric strain.

Note that e_V and E_{slip} in equations (1)–(3), are computed from the local changes to Mg bonds inside the dislocation core, compared to the defect-free bulk Mg. Originally, the misfit approximation for solute/dislocation interaction energy was applied to obtain the interaction energy map of basal dislocations in Mg with Al solutes. Al does not alter the basal dislocation core structure. Therefore, the core geometry of the relaxed dislocation in pure Mg was used to compute e_V and E_{slip}. In this paper, we have shown that the addition of Y solutes dramatically changes the dislocation geometry.

To obtain the interaction energy map, we consider the pure Mg $\langle c+a\rangle$ dislocation as the baseline for defining the Y solute positions. For each solute position, we then use the changed dislocation core which is obtained after the relaxation, calculate the interaction energy from Equation (5) at the location of the solute in the deformed core, and then assign that energy value to the solute position in the undeformed core. This way all of the changes in the dislocation core energy are packed into the solute/dislocation "interaction" energy and assigned to the initial location of the solute with respect to the $\langle c+a\rangle$ dislocation in pure Mg. This picture is consistent with the concept of a dislocation gliding in pure Mg and occasionally interacting with dilute solutes, and undergoing changes in the core geometry in the process. For atoms far away from the dislocation core, the continuum approximation of $-p(x,y)\Delta\nu$ is used, where $p(x,y)$ is the pressure field of the dislocation and $\Delta\nu$ is the misfit volume between the solute and the host. Note that $\Delta\nu$ is related to ε_b and equals $\varepsilon_b V_0$, where V_0 is the equilibrium atomic volume.

An additional step must be added when determining the interaction energy from the deformed solute cells. We are specifically interested in how the size difference interacts with volumetric strain resulting from a dislocation, where the difference in size is accounted for by the volume misfit. However, when determining the volumetric strain around the substituted solute atom in the deformed cell, the size difference is considered again in the strain exerted by the solute on its neighbors. As a result, this "bulk solute strain", which is simply determined as the strain resulting around the solute atom when it is relaxed in bulk Mg, needs to be removed from the total volumetric strain around the solutes when calculating interaction energy.

Before calculating the interaction energies, it is important to discuss another point that requires special attention, and that sets the solute $\langle c+a\rangle$ dislocation system in Mg apart from similar studies focused on basal dislocations: calculation of the pyramidal generalized stacking fault energy and the cross section of this surface, the γ-line. Obtaining the slip interaction energy, from Equation (6), requires an accurate representation of the γ-surface. Previous DFT studies do not show agreement between cross-sections of the generalized stacking fault energy surface and DFT relaxed dislocation core geometries for $\langle c+a\rangle$ dislocations dissociated along the pyramidal II plane [1,10,18]. Additionally, there have been no studies specifically examining the dissociation of these $\langle c+a\rangle$ dislocations in experimental samples. Relaxed core geometries show the dislocation dissociated into two stable $1/2\langle c+a\rangle$ partial dislocations, which would coincide with a local minimum halfway across the γ-surface in the $1/3[2\bar{1}\bar{1}3]$ direction, but γ-surface calculations do not have a minimum here. We find that a more reasonable representation of the generalized stacking fault energy can be obtained by spreading the displacement over a few layers of atoms above and below the stacking fault. This differs from the method generally used to calculate generalized stacking fault energies in that traditionally, the stacking fault is effectively treated as being a discrete plane, while this method considers a "stacking fault region." This method is based on a similar method introduced by Morris et al. [19] and has been recently shown to produce more consistent and feasible generalized stacking faults [20].

It should be noted that while the region around the stable stacking fault converges to a value, the unstable regions do not. This is not surprising, given our treatment of the stacking fault. As more atomic layers are considered, the regions of atoms that actually exhibit the stacking fault relative to each other shrink, while the regions of tilted atoms become larger (and by consequence, the tilt or "strain" over this region is diffused). For the extreme case, as the fully relaxed region nears the size of the stacking fault cell, the relaxed structure will more closely resemble simple shear strain on a bulk lattice. This is obviously not an accurate representation, so we limit the number of atomic layers to the number of layers needed to converge the area around the stable stacking fault in the generalized γ surface cross section.

This treatment is still reasonable for the unstable regions, because in a real dislocation, the regions that exhibit an unstable stacking fault are surrounded by stable (or metastable) regions, so we can expect this to at least give a reasonable upper bound for the energy of the unstable regions (the energy always drops as more atomic layers are considered and the cell relaxes more fully). However, the point still remains that we do not have a way to represent these unstable regions, though it stands to reason that this approximation of the unstable regions is at least as accurate as the traditional method, particularly since using the traditional method gives an upper bound for the entire generalized SFE. Finally, comparing the relative contributions of the misfit interactions reveals that the contribution of stacking fault misfit is small compared to the final interaction energy and the size misfit dominates the final interaction energy (see scales of plots in Fig. 4 for relative interaction energy contributions).

As a result, even moderate changes will not have a strong relative impact on the final interaction energy. Therefore, for the purpose of calculating the interaction energy, considering the upper bound of energy in the unstable regions of the γ-surface is a reasonable assumption.

Fig. 5 shows the interaction energy map between Y solutes and the $\langle c+a\rangle$ edge dislocation in Mg, considering the subtleties of core structure change and stacking fault calculations, as explained above. Next, we use this energy map as input to a solute strengthening model to predict the change in CRSS for pyramidal II glide of the $\langle c+a\rangle$ dislocations.

5. Predictions of the CRSS

We use the strengthening model introduced by Leyson et al. Details of this model are explained in Refs. [4,21,22]. The model's central idea is that an initially straight dislocation in a random field of solutes will bow out to lower its energy by finding regions of favorable solute fluctuations. However, in doing so, the length of the dislocation increases, which is associated with a cost in elastic line energy of the dislocation. The total energy is optimized at some critical values for the roughening amplitude of the bowing

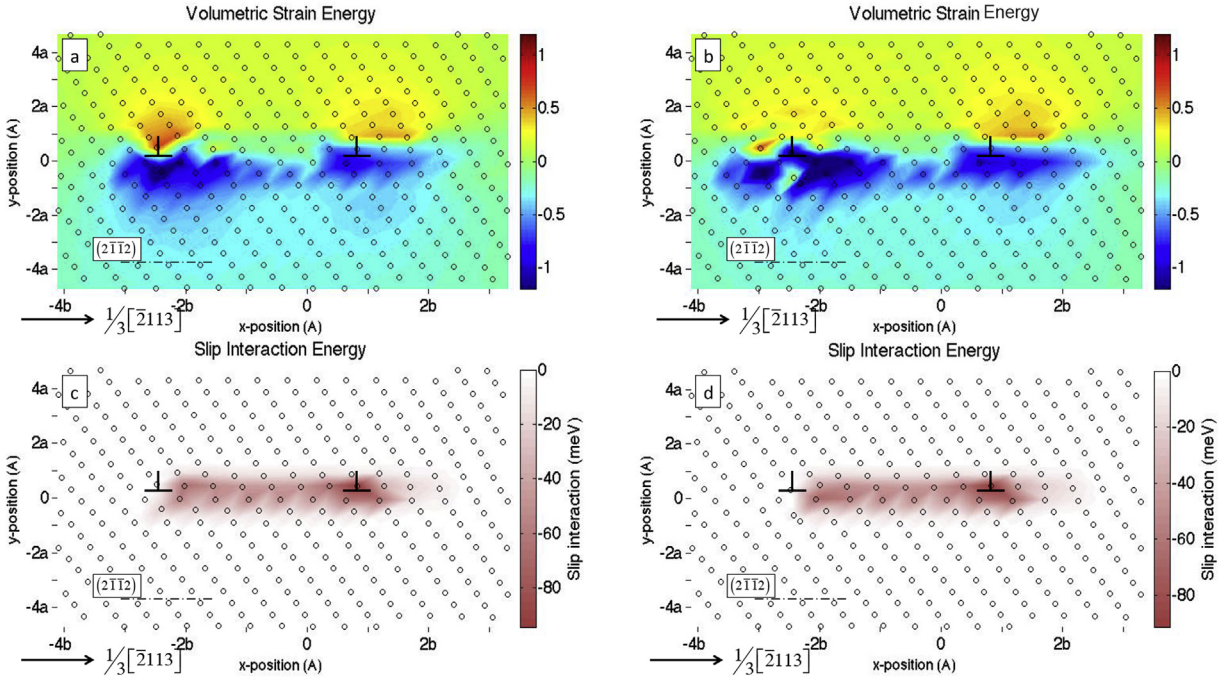

Fig. 4. Plots of the contributions to the interaction energy of volumetric strain in (a) and (b) and slip interaction energy in (c) and (d) for the $\langle c+a \rangle$ dislocation. Parts (a) and (c) show the interaction energies using the pure Mg dislocation, while parts (b) and (d) show the interaction energies calculated for the dislocation with a solute at position 20. Notice that the local slip environment is not changed nearly as drastically as the volumetric strain with the addition of a solute.

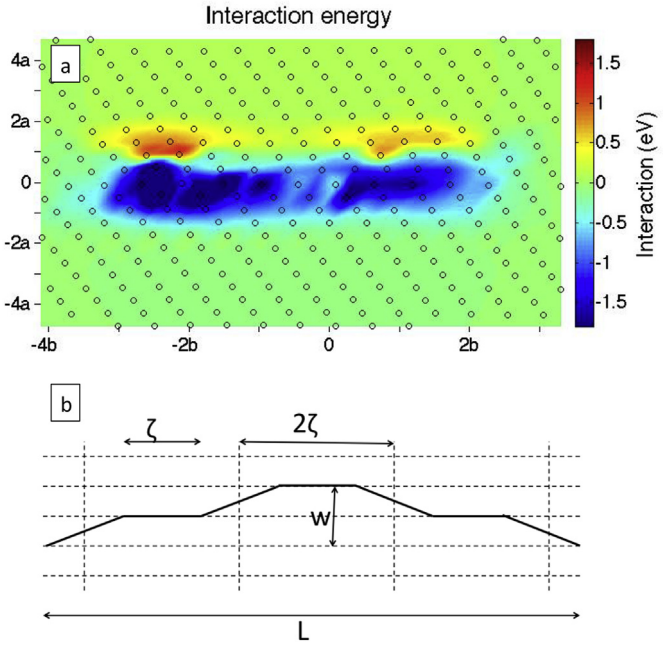

Fig. 5. All of the information needed to apply the solid solution strengthening model. The top plot shows the final interaction energy map that considers directly calculated interaction values for solutes immediately within the dislocation core region. The schematic on the bottom shows how the dislocation is described in Leyson et al.'s strengthening model. The dislocation with a length of L is separated into segments of ζ, which bow out over length w due to favorable interactions with solutes.

dislocation w_c and critical segment lengths ζ_c. Table 1 shows the critical roughening amplitudes and segment lengths for strengthening of the $\langle c+a \rangle$ dislocation by Y. To determine the role of core changes by Y, we also calculated the interaction energy map ignoring all the shape changes, by applying the original misfit approximation to the $\langle c+a \rangle$ dislocation core in pure Mg. We call these cases "modified" and "unmodified" cores respectively. Moreover, we include the strengthening parameters for basal slip as well for comparison. The Y interaction energy map with the basal dislocation is computed by applying the misfit approximation to this dislocation core, and again ignoring any changes to the basal dislocation core structure.

We use a line tension of $\Gamma = 4.0\,\text{eV nm}{-1}$ for basal edge dislocations, based on molecular statics calculations an EAM Mg [9]. For $\langle c+a \rangle$ dislocations, we calculate the line energy of the dislocation using an updated MEAM potential [1]. A dislocation is relaxed in the center of a bulk slab of Mg, and the excess energy of the dislocation (elastic and core energy) is determined as a function of the radius away from the dislocation. The line tension is then determined by removing the elastic energy from this total excess energy, so that the remaining core energy levels off at the line tension beyond the core radius. Using this method, the line tension of a $\langle c+a \rangle$ dislocation was found to be 17.5 eV nm^{-1}.

As shown previously for the basal dislocation [9], there are two critical roughening amplitudes that minimize the total energy. The strength is then dominated by the configuration with the highest stress required to unpin the dislocation. The reason for existence of two critical configurations is the large separation of the partials. Closer to the SF plane, the large partial separation means a small roughening amplitude decorrelates the solute fluctuations inside the dislocation partials. This small roughening amplitude is not sufficient to significantly decorrelate solutes farther from the core, resulting in a second energy minimum at a larger roughening amplitude. It is not surprising that the $\langle c+a \rangle$ dislocation also exhibits two energy minima, as the partial separation is even larger than that in the basal dislocation. This underlines the importance of having accurate, detailed structures of the dislocations. It also again highlights the significant impact of the solutes on the dislocation, as certain Y solute positions change the separation between the

Table 1
Major strengthening parameters found for a basal dislocation, the unmodified pyramidal II dislocation, and the pyramidal II dislocation modified with directly calculated interaction energies near the dislocation. ΔE_b is the energy barrier for slip, and τ_{y0} is the 0 K strengthening effect. The c term is present in each of the reported values because these are normalized by concentration. Values are shown for both dislocation configurations (short and long range) for each system.

Strengthening Parameters	w_c (nm)	$\zeta_c c^{1/3}$ (nm)	$\Delta E_b/c^{1/3}$ (eV)	$\tau_{y0}c^{2/3}$ (MPa)
Basal Config. 1	0.7988	3.9209	1.5155	381
Basal Config. 2	2.8755	15.3835	5.0060	89
Pyr2 unmod Config. 1	0.3045	0.6390	4.1829	8885
Pyr2 unmod Config. 2	2.7404	7.5816	28.5544	568
Pyr2 mod Config. 1	0.6090	1.3215	8.0901	4154
Pyr2 mod Config. 2	2.4359	6.2081	27.5530	752

partials.

For each dislocation, configuration 1 is associated with short range behavior, and has a high zero temperature yield stress (τ_{y0}), and a relatively low energy barrier (ΔE_b). Configuration 2 is associated with longer range behavior, has a low zero temperature yield stress and a larger energy barrier. In a real system, the dislocation would have to overcome both energy barriers, and the larger of the two dominates the strength and is thus chosen in the calculations.

Fig. 6 shows the temperature and solute concentration dependence of the solute strengthening effect $\Delta\tau_y$ for basal and pyramidal $\langle c+a\rangle$ dislocations. Fig. 6a illustrates the temperature dependence of $\Delta\tau_y$ of basal and pyramidal II slip systems separately, while (b) shows the ratio between the pyramidal and basal values. As mentioned previously (c.f. Table 1), there are two characteristic dislocation configurations that minimize the energy. These are represented in Fig. 6a separately, using dashed and solid lines. Note that the second critical roughening amplitude for the pyramidal dislocation always requires smaller stress levels to unpin the dislocations and thus does not become relevant until higher temperatures, beyond the range considered with this model. On the other hand, the second configuration for the basal dislocation dominates the strength around 600K. Part (b) shows that the ratio of the $\Delta\tau_y$ for pyramidal II and basal modes increases slightly at first, but then decreases above about 600 K, corresponding to where the second configuration becomes dominant for the basal dislocation. Above this temperature, the strengthening continues to decrease faster for pyramidal slip than for basal as the basal strengthening levels off. This may change at higher temperatures when the second configuration becomes dominant for pyramidal slip as well, but the high temperature regime could violate some of the basic assumptions made in the solute strengthening model and therefore is not considered here.

Fig. 6 (c) and (d) show the effect of solute concentration on $\Delta\tau$ pyramidal and basal dislocations and their ratio at T = 300K respectively. The ratio of pyramidal to basal strengthening decreases with increasing solute concentration, implying the basal mode is strengthened more than the pyramidal II, leading to a more isotropic plastic deformation and consequently better ductility.

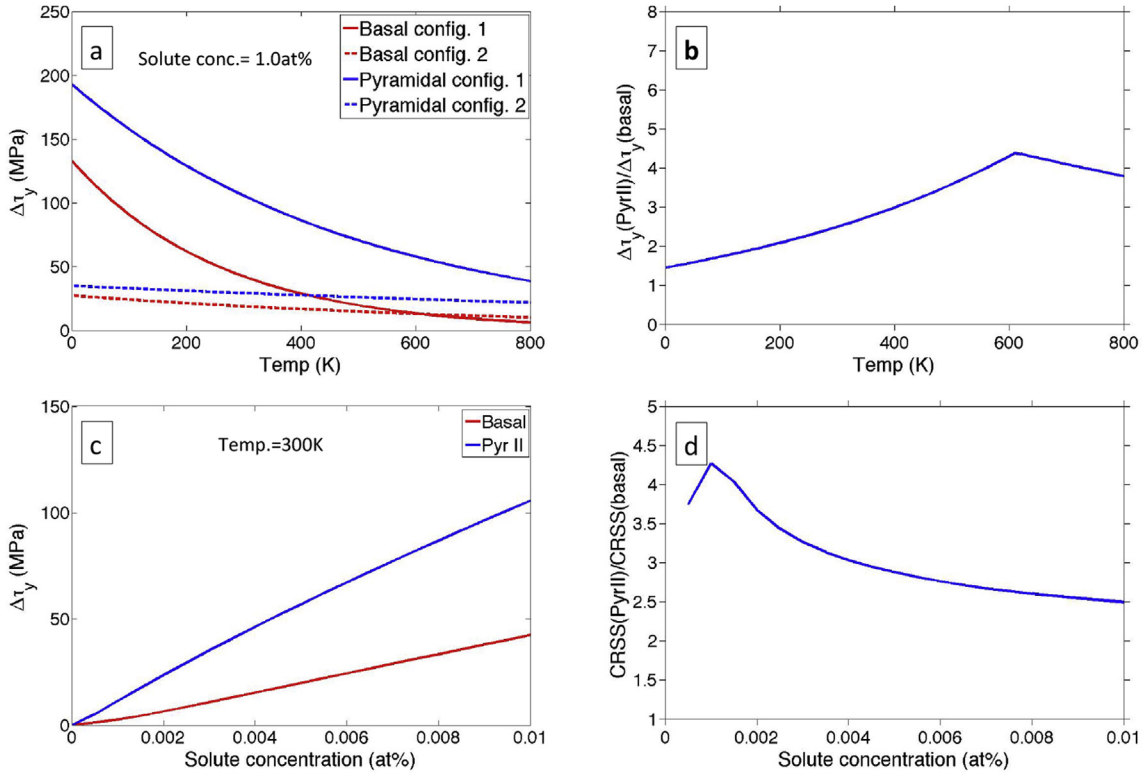

Fig. 6. The strengthening effect of solutes as a function of temperature (a) and solute concentration (c). Parts (b) and (d) show the ratio between the strengthening effects on pyramidal and basal slip as a function of temperature and concentration, respectively. (a) shows the strengthening effects on two dislocation configuration that minimize the total energy, shown as solid and dashed lines. Parts (a) and (b) illustrate how a change in the dominant dislocation configuration can significantly affect the ratio between strengthening effects on pyramidal and basal slip. The two configurations are evident in the concentration plot as well, though they are not included here for the sake of clarity.

However it is important to note that before comparing to experiments, the CRSS for each mode in pure Mg should be added to $\Delta\tau$. Fig. 7 shows the final CRSS values for pyramidal and basal slip (the sum of $\Delta\tau_y$ shown in Fig. 6 and the CRSS in pure Mg, which is taken as 0.5 MPa for basal [23] and 62 MPa for pyramidal [24] at 300 K). As Fig. 7 indicates, despite the fact that at each concentration, the CRSS for pyramidal slip is larger than that for basal slip, the ratio is dominated by the large discrepancy in pure Mg, and as a result adding yttrium still reduces the CRSS ratio by more than an order of magnitude.

6. Discussion and conclusions

We have computed the structure and solute interaction energies of an edge $\langle c+a\rangle$ dislocation in Mg, using DFT calculations. First, we showed that Y solutes changed the core geometry and posed challenges to the computation of a well-defined interaction energy map. We approached this problem by approximating the interaction energy through the misfit approach, proposed by Yasi et al. [3], but with a different core geometry associated to each solute position. The modified dislocation cores were calculated directly by optimizing the core in the presence of Y, at the corresponding position, with DFT. This result is very important for the study of deformation behavior in metals in general since it could potentially be applied to any slip system. While it could even be applied to basal systems, the deformation is small enough to be neglected for basal dislocations, making it unnecessary to account for the shape change. However, this method would be more useful when considering more complex slip systems. In particular, it can be used to more accurately examine the behavior of pyramidal slip in any HCP metal.

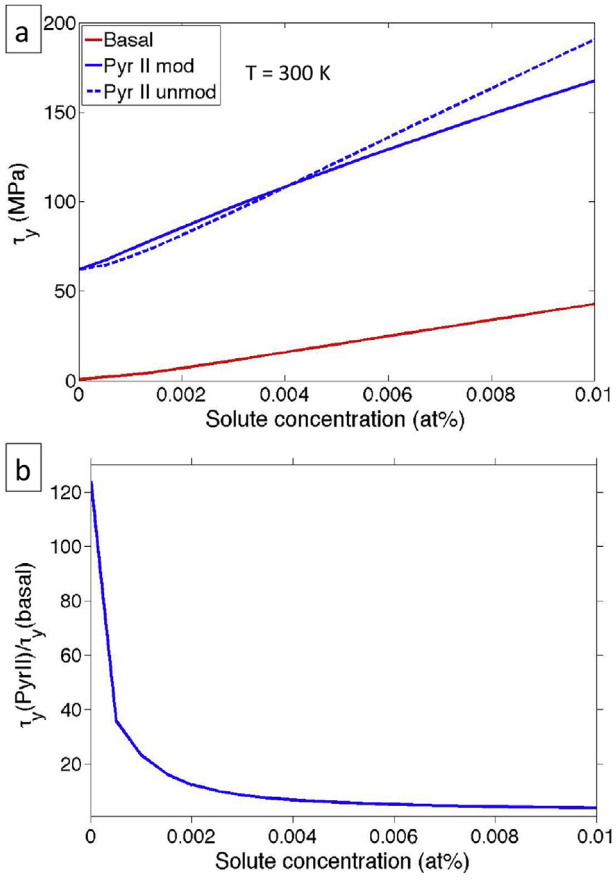

Fig. 7. The total CRSS as a function of solute concentration (a) and the ratio of pyramidal to basal CRSS (b). This CRSS includes our calculated strengthening effect and the room temperature CRSS of pure Mg. The CRSS ratio illustrates how even though the strengthening is higher for pyramidal slip than basal, the addition of yttrium solutes should still reduce the CRSS ratio, and thus improve the ductility of the metal.

Next, we used this accurate interaction energy map in a solid solution strengthening model introduced by Leyson et al. [4] to determine the relative strengthening effect of Y solutes on basal vs. non-basal $\langle c+a\rangle$ dislocations. We found that ratio between CRSS for $\langle c+a\rangle$ slip and that for the basal slip reduces significantly as Y concentration increases from zero to 1 at% at room temperature, resulting in reduced plastic anisotropy in Mg-Y alloys, which is consistent with experimental observations of improved room temperature ductility in these alloys. However, a fixed concentration of Y increasingly strengthens pyramidal II more than the basal mode with increased temperature.

Next, we compare our results to recent findings by Ando et al. who have measured the stress required for second order pyramidal slip to occur [24]. In that study, the Mg-Y single crystals were stressed along the c-axis, and so the CRSS can be determined by simply multiplying their reported yield stress by the appropriate Schmid factor. As mentioned above, it is important to note that our model only calculates the change in strength from solutes, so in order to get an accurate representation of the CRSS, the CRSS of pure Mg must be included. We used values of 62 MPa at 300K and 40 MPa at 473 K reported in Ref. [24]. Using a solute concentration of 0.5%, we predict CRSS values of 114 MPa and 60 MPa at 300 K and 473 K, respectively, compared to the experimental values of 112 MPa and 56 MPa, overall showing very good agreement.

We emphasize that the relative solute strengthening of pyramidal and basal modes is only one piece of the greater puzzle of alloying effects on plasticity of Mg alloys. For example, a recent molecular dynamics study by Wu and Curtin [17] reveals that the DFT-predicted core for the $\langle c+a\rangle$ edge dislocation has an easy glide mode on the pyramidal II planes, but undergoes a thermally-activated, stress-dependent core transition, where the original $\langle c+a\rangle$ dissociates along the basal planes, and thus becomes immobile and contributes to the high work hardening rate during $\langle c+a\rangle$ slip. What we present in this paper only considers the effect of solutes on the easy glide mode. Another important issue is how alloying elements affect this core transition. Moreover, effect of alloying on stress and temperature dependence of the screw components' cross slip process should be quantified and compared with those of the thermally-activated process of core transitions in the edge components. There are also other mechanisms that are often significant during deformation in Mg alloys, such as twinning modes.

Nonetheless, systematic studies of individual deformation modes, such as the one presented here, are useful in providing a fundamental understanding of alloying effects on deformation behavior, towards quantitative and predictive design of new alloys.

Acknowledgments

We acknowledge the support of this work by the NSF - GOALI Grant No. 1309687 and NSF DMR-1709236. Computational resources were provided by the General Motors High Performance Computing Center and in part by the Ohio Supercomputer center.

References

[1] Z. Wu, M.F. Francis, W.A. Curtin, Magnesium interactomic potential for simulating plasticity and fracture phenomena, Model. Simulat. Mater. Sci. Eng. 23 (2015).
[2] G.I. Taylor, Plastic strain in metals, J. Inst. Met. 62 (1938).
[3] J.A. Yasi, L.G. Hector Jr., D.R. Trinkle, First-principles data for solid-solution strngthening of magnesium: from geometry and chemistry to properties,

Acta Mater. 58 (2010) 5704–5713.
[4] G.P.M. Leyson, L.G. Hector Jr., W.A. Curtin, Solute strengthening from first principles and application to alluminum alloys, Acta Mater. 60 (2012) 3873–3884.
[5] M. Ghazisaeidi, L.G. Hector Jr., W.A. Curtin, Solute strengthening of twinning dislocations in mg alloys, Acta Mater. 80 (2014).
[6] J.A. Yasi, L.G. Hector Jr., D.R. Trinkle, Prediction of thermal cross-slip in magnesium alloys from a geometric interaction model, Acta Mater. 60 (2012).
[7] J.A. Yasi, L.G. Hector Jr., D.R. Trinkle, Prediction of thermal cross-slip in magnesium alloys from direct first-principles data, Acta Mater. 59 (2011).
[8] S. Sandloebes, S. Zaefferer, I. Schestakow, S. Yi, R. Gonzalez-Martinez, On the role of non-basal deformation mechanisms for the ductility of mg and mg-y alloys, Acta Mater. 59 (2) (2011).
[9] G.P.M. Leyson, L.G. Hector Jr., W.A. Cutin, First-principles prediction of yield stress for basal slip in mg-al alloys, Acta Mater. 60 (2012) 5197–5203.
[10] M. Ghazisaeidi, First-principles core structures of $\langle c+a \rangle$ edge and screw dislocations in mg, Scripta Mater. 75 (2014).
[11] G. Kresse, J. Furthmuller, Efficient iterative scheemes for ab initio total energy calculation using a plane-wave basis set, Phys. Rev. B 54 (1996).
[12] G. Kresse, J. Hafner, Ab initio molecular dynamics for liquid metals, Phys. Rev. B 47 (1993).
[13] J.P. Perdew, Y. Wang, Accurate and simple analytic representation of the electron-gas correlation energy, Phys. Rev. B 45 (1992).
[14] S. Vannarat, M.H.F. Sluiter, Y. Kawazoe, First-principles study of solute-dislocation interaction in aluminum-rish alloys, Phys. Rev. B 64 (22) (2001).
[15] B. Yin, Z. Wu, W.A. Curtin, First-principles calculations of stacking fault energies in mg-y, mg-al, and mg-zn alloys and implications for $\langle c+a \rangle$ activity, Acta Mater. 136 (2017).
[16] C.S. Hartley, Y. Mishin, Characterization and visualization of the lattice misfit associated with dislocation cores, Acta Mater. 53 (2005) 1313–1321.
[17] A. Wu, W.A. Curtin, The origins of high hardening and low ductility in magnesium, Nature 526 (2015) 62–67.
[18] Z. Pei, L.F. Zhu, M. Friak, S. Sandloebes, et al., Ab initio and atomistic study of generalized stacking fault energies in mg and mg-y alloys, N. J. Phys. 15 (4) (2013).
[19] J.R. Morris, J. Scharff, K.M. Ho, D.E. Turner, Y.Y. Ye, M.H. Yoo, Prediction of $\{11\bar{2}2\}$ hcp stacking fault using a modified generalized stacking fault calculation, Philos. Mag. A 76 (1997).
[20] B. Yin, Z. Wu, W.A. Curtin, Comprehensive first-principles study of stable stacking faults in hcp, Acta Mater. 123 (2017).
[21] G.P.M. Leyson, W.A. Cutin, L.G. Hector Jr., C. Woodward, Quantitative prediction of solute strengthening in aluminum alloys, Nat. Mater. 9 (9) (2010).
[22] C. Varvenne, G.P.M. Leyson, M. Ghazisaeidi, W.A. Curtin, Solute strengthening in random alloys, Acta Mater. 124 (2017).
[23] H. Tonda, S. Ando, Effect of temperature and shear direction on yield stress by $\{11\bar{2}2\}\langle 1\bar{1}23 \rangle$ slip in hcp metals, Metall. Mater. Trans. 33 (3) (2002).
[24] S. Ando, A. Kodera, T. Yagi, M. Tsushida, Alloying effects on non-basal slips in magnesum single crystals, in: Materials Science and Technology Conference and Exhibition 2013, 2, 2013, pp. 1449–1454. MST2013.